Research Article

Evaluation of anti-tuberculosis activity of some oxotitanium(IV) Schiff base complexes; molecular docking, dynamics simulation and ADMET studies

Monir Uzzaman[1] · **Md. Junaid**[2] · **Mohammad Nasir Uddin**[1]

Received: 22 December 2019 / Accepted: 30 March 2020 / Published online: 11 April 2020

Abstract
Schiff base and their metal complexes have a wide range of chemical, biological, and medicinal applications including tuberculosis. Multi-drug resistant and extensively drug-resistant tuberculosis indicating the importance of new potent agent for tuberculosis. Herein, we report the optimization of some bis-unsymmetric dibasic tetradentate N_2O_2 oxotitanium (IV) Schiff base complexes based on density functional theory. All the compounds were optimized at B3LYP/6-31G (d) level of theory. Frontier molecular orbital features, thermodynamic properties, dipole moment, electrostatic potential were investigated. All the compounds were subjected for molecular docking against beta-lactamase (BlaC) protein (3ZHH) to search binding affinity, binding mode(s). Molecular dynamics simulation was performed for the best bounded complex (C3) to observe the stability of protein-drug complexes. It was observed that all compounds were thermodynamically stable, while the addition of metal oxide increases thethermochemical stability, dipole moment, and chemical softness. Molecular docking and non-bonding interactions result disclosed the significant binding and interactions of some compounds with the receptor protein. ADMET calculations suggesting, all the compounds are non-carcinogenic and safe for biological use. Finally, this study may be helpful to design of new anti-tuberculosis agent.

✉ Monir Uzzaman, monircu92@gmail.com | [1]Department of Chemistry, University of Chittagong, Chittagong 4331, Bangladesh. [2]Molecular Modeling Drug-Design and Discovery Laboratory, Pharmacology Research Division, Bangladesh Council of Scientific and Industrial Research, Chattogram 4220, Bangladesh.

SN Applied Sciences (2020) 2:880 | https://doi.org/10.1007/s42452-020-2644-0

Graphic abstract

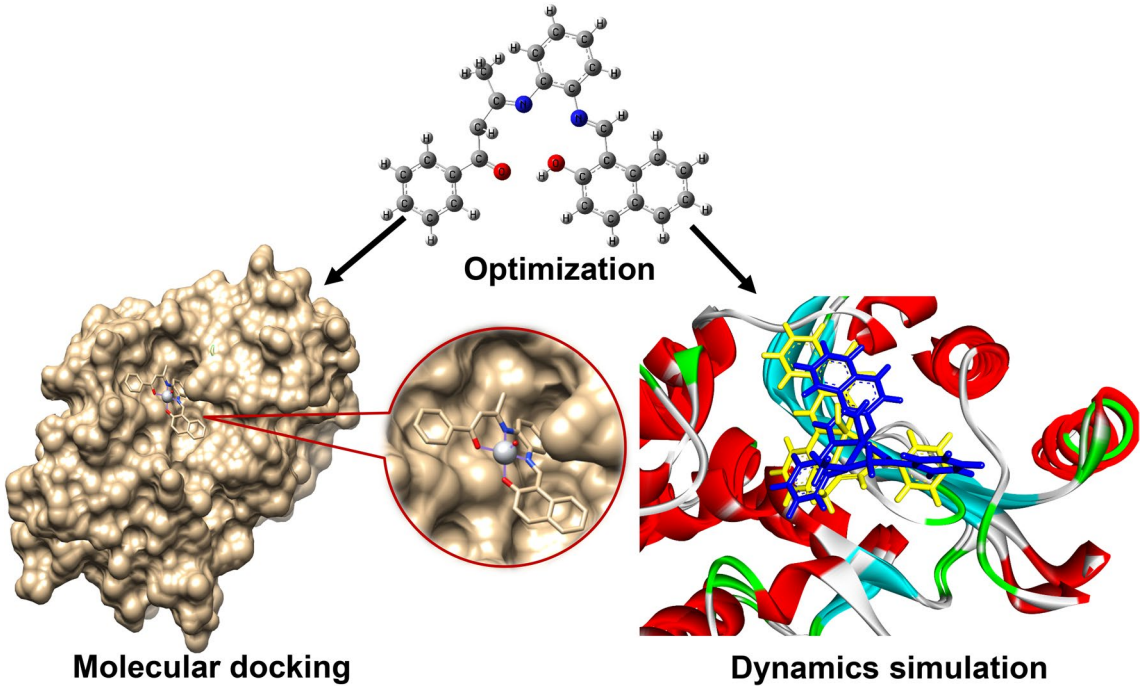

Keywords Tuberculosis · Schiff base · Molecular docking · Molecular dynamics · ADMET

1 Introduction

Mycobacterium tuberculosis (MTB) is a type of pathogenic bacteria as resulting the infectious diseases of tuberculosis (TB) in human [1]. Multidrug-resistant (MDR) and extensively drug resistant (XDR) TB are threatening the treatment of TB [2, 3]. Though different anti-tuberculosis drugs are available in the market, MDR-TB and XDR-TB indicating the importance of the discovery of new drugs against TB [3–5]. Due to the simple synthesis method, coordination variety, catalytic, medicinal and biological applications Schiff base ligands and their metal complexes achieved much attention [6]. Many of the Schiff base metal complexes act as antifungal, antibacterial [7], antiviral [8], herbicidal [9], analgesic [10], anti-inflammation [11, 12], antioxidant [6, 13], antitumor [14, 15], anticancer [16, 17], antitubercular [18–20] agent. Previously, many investigations have been demonstrated that, Schiff base with aromatic and hetarocyclic ring coordinated with transitional metals show potential activity against MTB and different microorganisms [18, 20–24], suggesting new possible candidate to break the resistant of MTB. Synthesis, characterization and biomedical application of our investigated ligands and complexes were reported in our previous work [25].

In this investigation, we report the optimization and beta-lactamase inhibition pathway of some bis-unsymmetric dibasic tetradentate N_2O_2 oxotitanium(IV) Schiff base complexes utilizing molecular docking calculation and dynamics simulation. Thermodynamic energy levels, HOMO (highest occupied molecular orbital), LUMO (lowest unoccupied molecular orbital), hardness, softness, chemical potential, electrostatic potential, nonbonding interactions, and pharmacokinetic properties have been studied to evaluate their chemical and biological properties.

2 Methods and computational details

2.1 Geometry optimization of all Schiff base and their metal complexes

Gaussian 09W program package was used to draw and optimize all the structures [26]. Quantum mechanical (QM) methods have greater attention on the calculation of thermodynamic properties, molecular orbital features, dipole moment, atomic partial charge, molecular electrostatic potential and as well as interpretation of different types of interactions [27]. All the compounds were optimized using density functional theory (DFT) with Becke's (B) [28]

exchange functional combining Lee, Yang and Parr's (LYP) correlation functional [29] under Pople's 6-31G (d) basis set which has amply been proven to give very good ground state geometries [30]. Dipole moment, electronic energy, enthalpy, free energy, and electrostatic potential were calculated for all compounds.

Frontier molecular orbital features HOMO, LUMO were calculated at the same level of theory. For each of the compounds, HOMO–LUMO gap, hardness (η), softness (S), and chemical potential (μ) were calculated from the energies of frontier HOMOs and LUMOs as previously reported [31] considering Parr and Pearson interpretation [32, 33] of DFT and Koopmans theorem [34].

$$\eta = \frac{[\varepsilon\text{LUMO} - \varepsilon\text{HOMO}]}{2}; \quad \mu = \frac{[\varepsilon\text{LUMO} + \varepsilon\text{HOMO}]}{2}; \quad S = \frac{1}{\eta}$$

2.2 Molecular docking analysis

Three-dimensional crystal structure of full-length BlaC (beta-lactamase) (PDB id: 3ZHH) was retrieved in PDB format from the protein data bank [35]. After that, the structure was prepared by deleting water molecules and adding hydrogen atoms utilizing PyMol (version 1.3) software packages, which was subsequently subjected to energy minimization using the steepest descent and conjugate gradient technique to eliminate bad contacts of protein atoms implementation of Swiss-PDB Viewer (version 4.1.0). To understand the binding mechanism between protein–ligand molecules, molecular docking analysis was done by using PatchDock web server [36] based on shape complimentary principles. Further, the output provided by PatchDock is filtered by FireDock [37]. FireDock is an important web server that is highly useful in the flexible refinement and scoring of protein–protein docking solutions. FireDock functions to optimize the side chain conformations and rigid body orientations and hence provides a better refinement. Its user-friendly interface and speed of processing drives it amongst the top docking servers available. Using UCSF Chimera [38] and Accelrys Discovery Studio 4.5 software for the binding patterns analysis of the resulting docked complexes.

2.3 Molecular dynamics simulation

The predictions from molecular docking study was validated using molecular dynamics simulation by means of the YASARA Dynamics software [39]. The AMBER14 force field [40] was employed for this study, which is widely used to describe a macromolecular system. In addition, the transferable intermolecular potential 3 points (TIP3P) water model was applied by adding $Cl^-$and/or Na^+ ions, where the total solvent molecules were 52,672 with a density of 1.026 gm/cm^3. To perform the simulation, the periodic boundary condition was incorporated, where the box size $80.56 \times 80.56 \times 80.56$ Å^3. The minimization of initial energy for each simulation system was performed by the simulated annealing method, via steepest gradient approach (5000 cycles). Again, molecular dynamics simulations were performed utilizing the PME methods to designate long-range electrostatic interactions at a cut off distance of 8 Å at physiological conditions (298 K, pH 7.4, 0.9% NaCl) [41]. A multiple time step algorithms together with a simulation time step interval of 2.50 fs was selected [42]. Molecular dynamics simulations were performed for 10 ns long at a constant pressure and Berendsen thermostat, and MD trajectories were saved every 10 ps for further analysis.

2.4 ADMET analysis

Absorption, metabolism and carcinogenicity of all compounds were predicted by utilizing AdmetSAR web server [43]. Structure data file and simplified molecular-input line-entry system strings were utilized throughout the conversion procedure.

3 Result and discussion

3.1 Thermodynamic properties

Molecular formula, molecular weight, electronic energy, enthalpy, Gibb's free energy, and dipole moment of all compounds were reported in Table 1. The spontaneity of a reaction and stability of reaction product can predict from Gibb's free energy, enthalpy, and electronic energy [44]. Where free energy plays an important role; greater negative values mention improved thermodynamic properties. Here, the free energy of all ligands and complexes are found negative which indicate their spontaneous binding and interactions [45]. Improved free energy, dipole moment, and chemical reactivity were observed due to addition of metal oxide. Improved free energies were observed for ligand L3 (−1301.696 Hartree) and its synthesized complex C3 (−2225.413 Hartree), hence suggesting a more stable configuration and spontaneous binding possibility.

In drug design, improved dipole moment can enhance hydrogen bond and non-bonded interactions in drug-receptor complexes which keep an important role to increase binding affinity. Polarity of a molecule increase with the increase of dipole moment [46]. The largest dipole moment was found for ligand L5 (4.437 Debye) and complex C1 (6.432 Debye). Therefore, increased dipole

Table 1 Stoichiometry, molecular weight, electronic energy, enthalpy, Gibb's free energy in Hartree, and dipole moment (Debye) of all ligands and complexes

Name	Stoichiometry	Molecular weight	Electronic energy	Enthalpy	Gibb's free energy	Dipole moment
L1	$C_{26}H_{22}N_2O_2$	394.46	−1263.52	−1263.52	−1263.59	3.64
L2	$C_{25}H_{20}N_2O_2$	380.44	−1224.25	−1224.23	−1224.31	0.82
L3	$C_{27}H_{22}N_2O_2$	406.47	−1301.61	−1301.61	−1301.69	2.29
L4	$C_{22}H_{20}N_2O_2$	344.41	−1109.93	−1109.93	−1110.01	3.09
L5	$C_{23}H_{22}N_2O_3$	374.43	−1224.43	−1224.43	−1224.52	4.44
C1	$C_{26}H_{20}N_2O_3Ti$	456.35	−2187.23	−2187.23	−2187.31	6.43
C2	$C_{25}H_{18}N_2O_3Ti$	442.29	−2147.94	−2147.94	−2148.02	4.55
C3	$C_{27}H_{20}N_2O_3Ti$	468.33	−2225.33	−2225.33	−2225.41	3.15
C4	$C_{22}H_{18}N_2O_3Ti$	406.26	−2033.58	−2033.58	−2033.65	4.80
C5	$C_{23}H_{20}N_2O_4Ti$	436.28	−2148.15	−2148.15	−2148.23	2.49

moment resulted in increased binding affinity with 3ZHH protein.

3.2 Frontier molecular orbital

The HOMO–LUMO energy gap, hardness (η), softness (S), and chemical potential (μ) of all ligands and complexes were tabulated in Table 2. The DOS plot and HOMO–LUMO energy gap of L3 and C3 are depicted in Figs. 1 and 2. The electronic absorption relates to the transition from the ground to the first excited state and mainly described by one electron excitation from HOMO to LUMO, which also help to know about chemical reactivity of the compounds [47]. The HOMO–LUMO energy gap significantly influence the chemical reactivity. Lower gap describes the high chemical reactivity, low kinetic stability [48–50]. Because of the addition of metal oxide, reduced energy gap and increased chemical reactivity were observed in metal complexes. Here, all complexes (except C1) show lower HOMO–LUMO gap than the ligands. Among the ligands and complexes, L3 and C4 show a lower HOMO–LUMO gap and higher softness values respectively. Where, C4 shows the highest chemical potential (−3.98 eV) value, which may contribute the higher chemical reactivity than others.

3.3 Molecular electrostatic potential

Molecular electrostatic potential (MEP) was calculated to forecast the reactive sites for electrophilic and nucleophilic attack. It also helps to interpret biological recognition process and hydrogen bonding interaction [51]. Red colour represents a maximum negative area which favourable site for electrophilic attack, blue colour indicates the maximum positive area which favourable site for nucleophilic attack and green colour represent the area of zero potential. MEP represent molecular size, shape as well as positive, negative and neutral electrostatic potential regions simultaneously in terms of colour grading [47]. From MEP map, the region having the negative potential are over electronegative atom (oxygen atoms) and having positive potential are over hydrogen atoms. In ligand, the maximum negative potentiality is −0.2363 a.u. in L2 (deepest red) for oxygen atoms and the maximum positive region localized on the H atoms have value + 0.1742 a.u. (deepest blue) in L4. Similarly, for complex, the highest negative value −0.7665

Table 2 Energy (eV) of HOMOs, LUMO, gap, hardness (η), softness (S), and chemical potential (μ) of all ligands and complexes

Name	εHOMO−1	εHOMO	εLUMO	Gap	η	S	μ
L1	−5.71	−5.40	−1.67	3.73	1.86	0.53	−3.53
L2	−5.75	−5.36	−1.63	3.73	1.86	0.53	−3.49
L3	−5.64	−5.23	−1.80	3.44	1.72	0.58	−3.51
L4	−5.80	−5.41	−1.61	3.80	1.90	0.53	−3.51
L5	−5.84	−5.26	−1.65	3.61	1.80	0.55	−3.45
C1	−5.75	−5.60	−2.12	3.48	1.74	0.57	−3.86
C2	−5.76	−5.52	−2.30	3.23	1.61	0.62	−3.90
C3	−5.76	−5.36	−2.18	3.17	1.59	0.63	−3.77
C4	−5.84	−5.44	−2.51	2.93	1.46	0.68	−3.98
C5	−5.70	−5.24	−2.10	3.14	1.57	0.64	−3.67

Fig. 1 Chemical structures of all ligands and their metal complexes

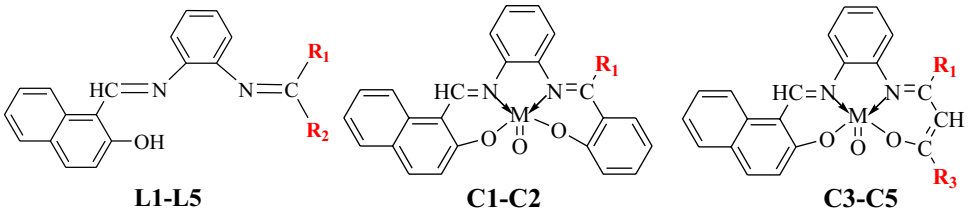

Name	R_1	R_2	R_3
L1/C1	$-CH_2CH_3$	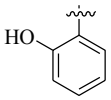	-
L2/C2	$-CH_3$	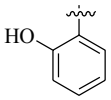	-
L3/C3	$-CH_3$	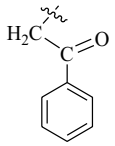	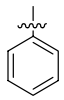
L4/C4	$-CH_3$	$-CH_2COCH_3$	$-CH_3$
L5/C5	$-CH_3$	$-CH_2COOCH_2CH_3$	$-OCH_2CH_3$

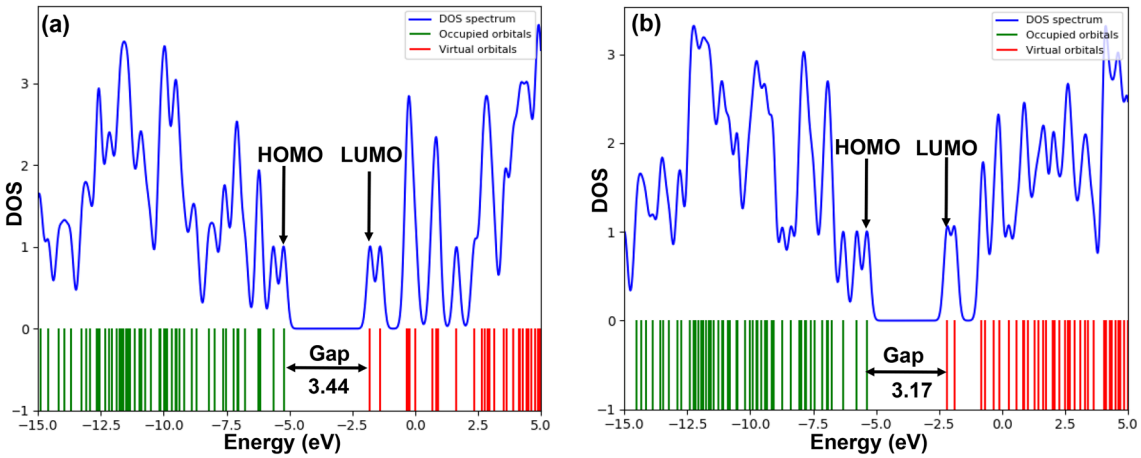

Fig. 2 DOS plot and HOMO–LUMO energy gap of **a** L3 and **b** C3

a.u. in C4 and the highest positive value is + 0.0899 a.u. in C3. The MEP surface provides a visual representation of the possible reactive site (Fig. 3).

3.4 Molecular docking analysis, and visualization

The investigation of binding properties of the designed compounds as β-lactamase inhibitor is accomplished by docking simulation by FireDock. Docking results predict that all compounds obtained binding affinity ranging from −7.4 to −12.3 kcal/mol. Binding affinities and ligand – protein interactions were summarized in Table 3. Among the ligands, L1 shows the highest binding affinity, similarly among the metal complexes, C3 exhibits high binding affinity. In addition, the previous studies proposed that all class A β-lactamases hydrolyzed β-lactam substrates through the nucleophilic assault started by Ser84 residue of the binding site [52]. Although, the other five

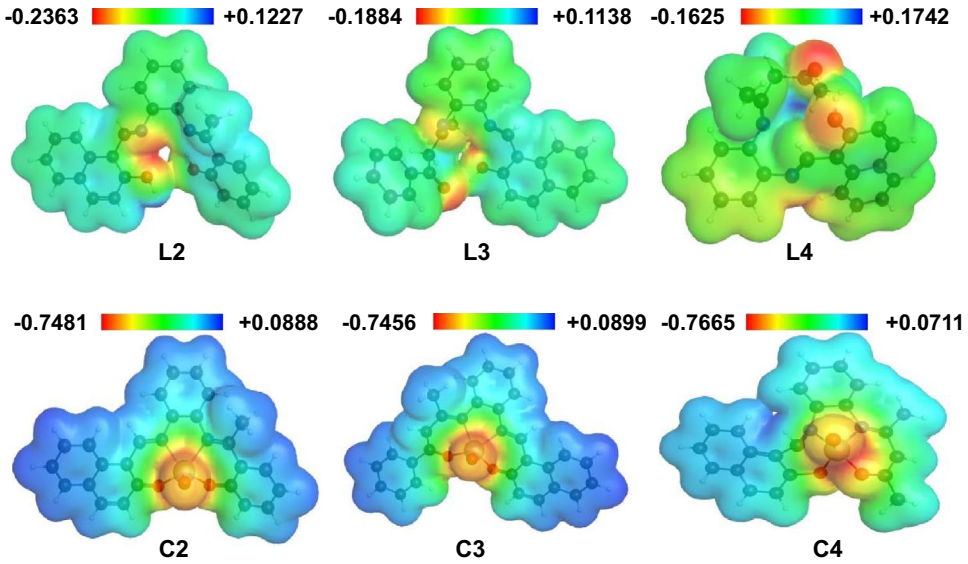

Fig. 3 Molecular electrostatic potential map of ligands L2, L3, L4 and their metal complexes (C2, C3, C4)

neighboring residues of the active site including Lys250, Thr251, Thr253, Ser142 and Gly144 make direct hydrogen bonding contact with the substrates [53]. In another study, it is also disclosed that Ile105 of BlaC acts as a 'gatekeeper' residue that regulates substrate accessibility to the enzyme active site [54]. In contrast, molecular docking study of the designed compounds shows that major residues of BlaC active site like Ile105 and Pro274 form hydrophobic interactions with the ligands by means of pi-alkyl bonding. Another important residue Arg220, which involved in electrostatic interaction with β-lactamases inhibitor, shows pi-cation interactions with L4, C3 and C4 compounds. Besides, C3 also showed pi-lone pair interaction with Thr237 residue. L2 which forms several amide-pi stacked with Thr237, Gly238, and Asp239 residue respectively. These study therefore suggest that the C3 has the strong interaction towards the binding site of BlaC (Fig. 4), however, whether this compound formed stable complex or not, molecular dynamics studies is performed along with the free form of BlaC enzyme.

3.5 Molecular dynamics simulation

In order to understand the binding mechanism, structural behavior and flexibility of the ligand molecules with the BlaC, we carried out 10 ns of MD simulation for C3 protein–ligand complex and apo form of protein. Two main parameters, Root Mean Square Deviation (RMSD) and Root Mean Square Fluctuations (RMSF) were subjected throughout the simulations.

According to the Fig. 5a free form of BlaC started the simulation at the RMSD value of 0.421 Å at 0 ns and reached to the highest peak of 1.21 Å at around 1.79 ns. It was then falling down to 0.80 Å at about 4.75 ns and again it increases significantly to 1.18 Å at around 5.5 ns and then gradually decreases up to 7.7 ns with a value of 0.77 Å. With regular fluctuations, it was then finally reached to 0.815 Å at 10 ns time.

Although, C3-BlaC complex exhibited an RMSD value of 0.43 Å in about 0 ns which is similar to its free form of BlaC and are stabled with 0.79 Å peak at around 1.2 ns. Afterwards, it gradually increased and reached to the highest peak of 1.32 Å at around 4.51 ns. It again maintained the stable conformation until 10 ns and finally reached 1.09 Å of RMSD value. From the RMSD analysis, it clearly revealed that C3-BlaC complex is more flexible than its free form of enzyme.

For describing the local changes along the protein chain, RMSF (Root Mean Square Fluctuation) is used in this study (Fig. 5b). On this plot, peaks demonstrate the areas of the protein that fluctuated most in the entire simulation period. The overall fluctuations of the RMSF of the ligands were found from a range of around 0.33–3.35 Å throughout the simulation. According to the Fig. 5b, it is observed that C3 increases flexibility of some residues in the protein. Highest fluctuations are observed in the several regions, ranging from 142–145, 175–180, 210–259, respectively. While, free form BlaC, revealed highest fluctuations at 28–54, 110–115 regions of the protein.

As a corollary, all analysis from the molecular dynamics simulations suggest that C3-BlaC is more stable than its free form of conformation, caused little conformational changes of protein, by undergoing little movement during the MD simulations (Fig. 6).

Table 3 Binding affinity and nonbonding interactions of all compounds after molecular docking with receptor protein 3ZHH

Compound	Binding affinity (kcal/mol)	Residues in contact	Interaction type	Distance (Å)
L1	− 10.8	Ile105	PA	4.999
		Ile 105	A	5.016
		Ile105	Psi	2.251
		Pro107	PA	4.553
		Glu166	Pa	4.688
		Thr237	Plp	2.923
L2	− 9.8	Ile105	PA	4.692
		Ile105	A	3.713
		Thr237	Aps	4.473
		Gly238	Aps	4.430
		Gly238	Aps	4.531
		Gly238	Aps	4.156
		Asp239	Aps	4.531
		Asp239	Aps	4.156
L3	− 9.5	Pro274	PA	4.501
		Ile105	PA	5.425
		Pro167	A	3.927
		Arg171	A	4.840
		Asp239	Pa	2.811
		Asp239	H	2.942
		Gly238	Plp	2.959
L4	− 8.6	Ile105	PA	4.633
		Ile105	PA	5.207
		Thr237	Aps	5.428
		Gly238	Aps	5.428
		Arg220	PC	4.602
		Thr237	H	2.272
L5	− 7.4	Pro274	PA	4.884
		Ile105	PA	5.270
		Thr237	H	2.698
C1	− 8.1	Tyr129	PA	5.449
		Ala218	PA	4.576
		Lys219	PA	4.179
		Ile105	A	4.731
		Pro107	A	4.484
		Pro107	A	4.284
		Glu276	Pa	4.753
		Glu276	Pa	4.223
C2	− 9.3	Pro167	PA	5.143
		Pro167	PA	4.892
		Pro274	PA	4.811
		Arg171	PC	2.377
		Gly238	Plp	2.445
C3	− 12.3	Ile105	PA	5.429
		Pro274	PA	4.552
		Arg220	PC	4.535
		Thr237	Plp	2.634
C4	− 8.0	Ile105	PA	5.397
		Ile105	A	4.563
		Thr237	Aps	4.718
		Gly238	Aps	4.718
		Arg220	PC	3.397
		Thr237	Plp	2.811
C5	− 8.9	Pro274	PA	4.478
		Pro274	PA	4.779
		Pro167	PA	5.128
		Gly238	Plp	2.840

H conventional hydrogen bond, *PC* Pi-cation, *Pa* Pi anion, *A* Alkyl, *PA* Pi-alkyl, *Psi* Pi-sigma, *Plp* Pi lone pair, *Aps* amide pi stacked

3.6 ADMET analysis

From ADMET calculation (Table 4), all the compounds are non-carcinogenic, show positive response for blood–brain barrier (BBB) and human intestinal absorption (HIA). They are P-glycoprotein non-inhibitor and show III category acute oral toxicity, where the inhibition can suppress the absorption, permeability and retention of the chemical compounds [55]. However, all the compounds show weak inhibitory property for the human ether-a-go-go-related gene (hERG). Inhibition of hERG can lead to long QT syndrome [56]. The rat acute toxicity level of all complexes (except C2) is higher resulting higher median lethal dose (LD_{50}) than the ligands.

4 Conclusion

In this investigation, five of the Schiff base ligands and their oxotitanium(IV) metal complexes have been studied to investigate their physicochemical and binding affinity with BlaC protein. From physicochemical data, complexes show the improved free energy, HOMO–LUMO gap, and dipole moment than the ligands due to the addition of metal oxide. Furthermore, C3 shows the highest free energy, binding affinity and remain stable inside the binding pocket of BlaC after the dynamic simulation. Nonbonding interaction result suggests that following residues Ile105, Pro224, Thr237, and Gly238 play a crucial role in ligand binding at the active pocket of BlaC. ADMET analyses also predict that all the compounds are non-carcinogenic and safe for oral administration. The above results ensure the binding possibility of all compounds

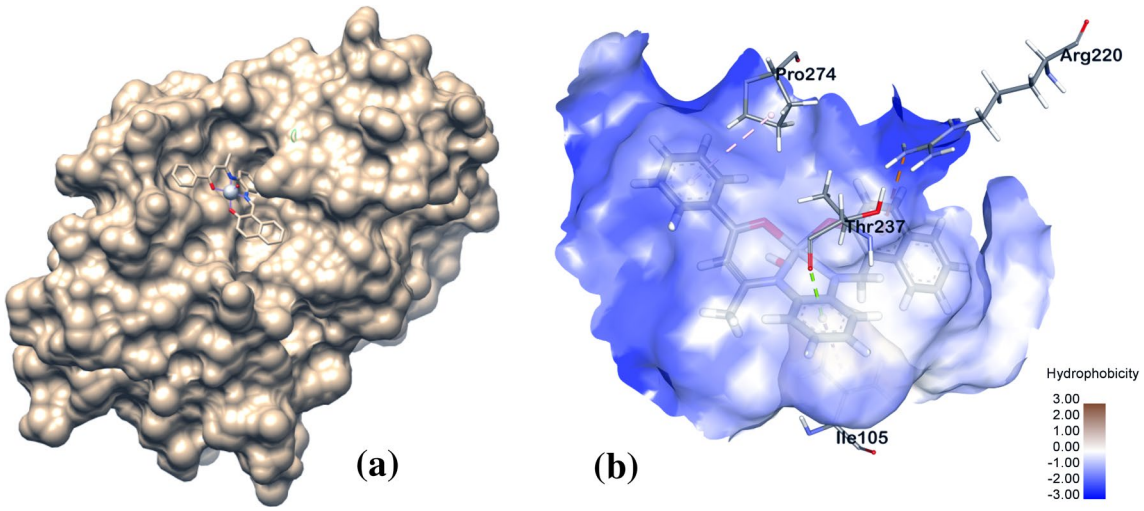

Fig. 4 **a** Predicted pose from docking analysis showed the binding orientation map of important amino acids for complex C3, **b** Hydrogen bond interaction (green color), including π–π stacking (pink color)

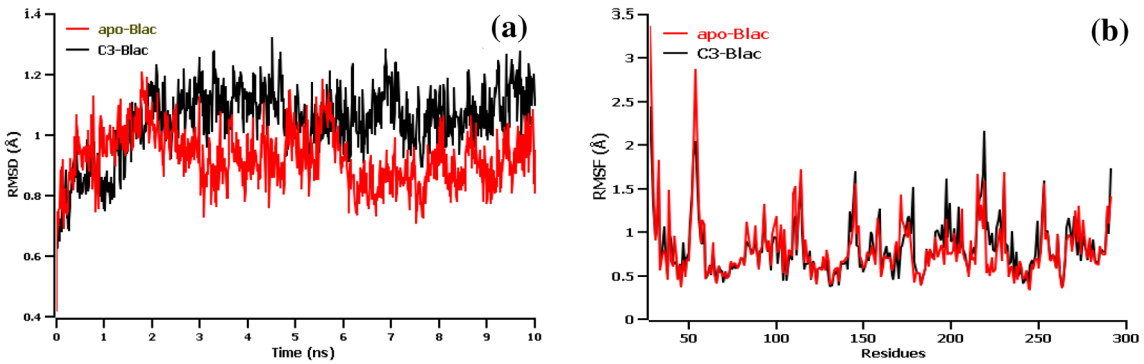

Fig. 5 **a** The time series of the RMSD of backbone atoms (C, Cα, and N) for a protein each docked complex, **b** The structural changes of protein by means of RMSF analysis. Here, black and red lines denote C3-BlaC complex and apo-Blac respectively

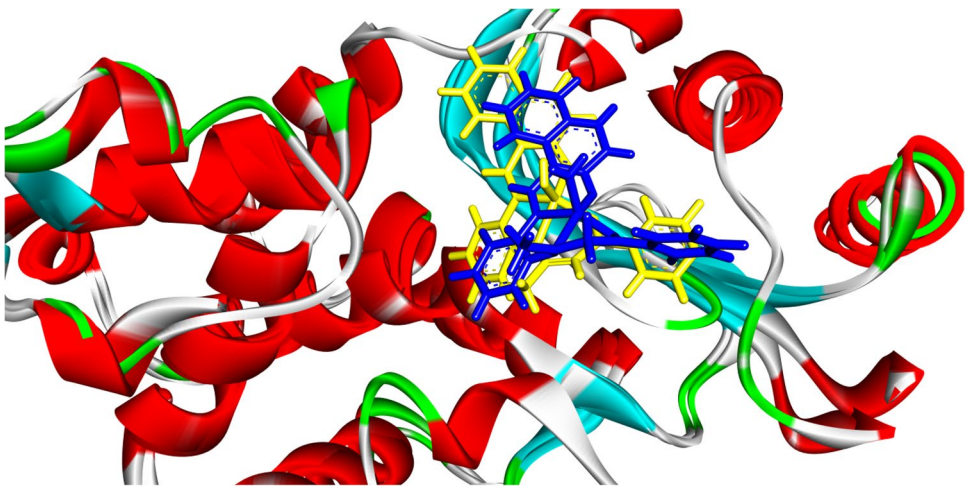

Fig. 6 Conformational changes of C3-BlaC complex. Here, stick model of ligand of yellow color represents the starting conformation of the complex, while blue color represents the conformation of last step in 10 ns long MD simulation

Table 4 Selected pharmacokinetic parameters of all ligands and complexes (Probability values related to each of the parameters are given in the parenthesis)

Name	BBB	HIA	P-glycoprotein inhibitor	CYP450 2C9 inhibitor	hERG	Carcinogen	Acute oral toxicity	Rat acute toxicity LD_{50} (mol/kg),
L1	+ (0.76)	+ (0.95)	NI (0.82)	I(0.71)	WI (0.82)	NC (0.57)	III	2.10
L2	+ (0.70)	+ (0.96)	NI (0.86)	I(0.61)	WI (0.88)	NC (0.62)	III	2.07
L3	+ (0.87)	+ (0.98)	NI (0.79)	I(0.53)	WI (0.83)	NC (0.65)	III	2.18
L4	+ (0.86)	+ (0.97)	NI (0.77)	NI(0.54)	WI (0.87)	NC (0.60)	III	2.24
L5	+ (0.70)	+ (0.95)	NI (0.87)	NI(0.53)	WI (0.85)	NC (0.60)	III	2.32
C1	+ (0.74)	+ (0.59)	NI (0.97)	NI(0.67)	WI (0.92)	NC (0.70)	III	2.35
C2	+ (0.73)	+ (0.62)	NI (0.97)	NI(0.70)	WI (0.93)	NC (0.74)	III	2.25
C3	+ (0.62)	+ (0.76)	NI (0.94)	I(0.51)	WI (0.93)	NC (0.68)	III	2.36
C4	+ (0.61)	+ (0.58)	NI (0.97)	NI(0.62)	WI (0.91)	NC (0.71)	III	2.36
C5	+ (0.75)	+ (0.88)	NI (0.99)	NI(0.64)	WI (0.93)	NC (0.87)	III	2.33

I inhibitor, *NI* non-inhibitor, *WI* weak inhibitor, *NC* non-carcinogenic

at the active site of beta-lactamase. Considering present investigation, L1, L2, L3, C2, C3, and C5 can be potent new possible candidate for better performance.

Acknowledgements Authors are thankful to Mohammad A. Halim, CEO, The Red-Green Research Centre for his valuable suggestion during molecular docking and dynamic simulation.

Author contributions MU performed all quantum mechanical calculation and data collection. MJ performed the dynamics simulation. MU and MJ wrote the manuscript draft. MNU revised the manuscript.

Funding This research was conducted by self-funding.

Compliance with ethical standards

Conflict of interest The authors declare that they have no conflict of interest.

References

1. Gordon SV, Parish T (2018) Microbe Profile: Mycobacterium tuberculosis: humanity's deadly microbial foe. Microbiology 164:437–439
2. Hugonnet J-E, Tremblay LW, Boshoff HI et al (2009) Meropenem-clavulanate is effective against extensively drug-resistant Mycobacterium tuberculosis. Science 80(323):1215–1218
3. Tessema B, Nabeta P, Valli E et al (2017) FIND Tuberculosis Strain Bank: a resource for researchers and developers working on tests to detect Mycobacterium tuberculosis and related drug resistance. J Clin Microbiol 55:1066–1073
4. Zager EM, McNerney R (2008) Multidrug-resistant tuberculosis. BMC Infect Dis 8:10
5. Rattan A, Kalia A, Ahmad N (1998) Multidrug-resistant Mycobacterium tuberculosis: molecular perspectives. Emerg Infect Dis 4:195
6. Uddin MN, Khandaker S, Amin S et al (2018) Synthesis, characterization, molecular modeling, antioxidant and microbial properties of some titanium (IV) complexes of schiff bases. J Mol Struct 1166:79–90
7. Bagihalli GB, Avaji PG, Patil SA, Badami PS (2008) Synthesis, spectral characterization, in vitro antibacterial, antifungal and cytotoxic activities of Co(II), Ni(II) and Cu(II) complexes with 1,2,4-triazole Schiff bases. Eur J Med Chem 43:2639–2649. https://doi.org/10.1016/j.ejmech.2008.02.013
8. Garg HG, Kaur N (1972) Synthesis of N'-substituted arylsulfonylpyrazoles, their anthelmintic activity, and the cytotoxicity of some hydrazides. J Med Chem 15:554–555
9. Ceyhan G, Celik C, Uruş S et al (2011) Antioxidant, electrochemical, thermal, antimicrobial and alkane oxidation properties of tridentate Schiff base ligands and their metal complexes. Spectrochim Acta Part A 81:184–198
10. Sondhi SM, Singh N, Kumar A et al (2006) Synthesis, anti-inflammatory, analgesic and kinase (CDK-1, CDK-5 and GSK-3) inhibition activity evaluation of benzimidazole/benzoxazole derivatives and some Schiff's bases. Bioorg Med Chem 14:3758–3765
11. Pandey A, Dewangan D, Verma S et al (2011) Synthesis of schiff bases of 2-amino-5-aryl-1, 3, 4-thiadiazole and its analgesic, anti-inflammatory, antibacterial and antitubercular activity. Int J Chem Tech Res 3:178–184
12. Hello KM, Shneine JK, Numan AA (2009) synthesis and biological activity of some barbituric acid derivatives via Schiff' s bases. Iraqi J Sci 50:423–430
13. Devi J, Yadav M, Jindal DK et al (2019) Synthesis, spectroscopic characterization, biological screening and in vitro cytotoxic studies of 4-methyl-3-thiosemicarbazone derived Schiff bases and their Co (II), Ni (II), Cu (II) and Zn (II) complexes. Appl Organomet Chem 33:e5154
14. Zhong X, Yi J, Sun J et al (2006) Synthesis and crystal structure of some transition metal complexes with a novel bis-Schiff base ligand and their antitumor activities. Eur J Med Chem 41:1090–1092. https://doi.org/10.1016/j.ejmech.2006.05.009
15. Qiao X, Ma Z-Y, Xie C-Z et al (2011) Study on potential antitumor mechanism of a novel Schiff Base copper(II) complex: Synthesis, crystal structure, DNA binding, cytotoxicity and apoptosis induction activity. J Inorg Biochem 105:728–737. https://doi.org/10.1016/j.jinorgbio.2011.01.004
16. Desai SB, Desai PB, Desai KR (2001) Synthesis of some schiff bases, thiazolidinones and azetidinones derived from 2, 6-diaminobenzo [1, 2-d: 4, 5-d'] bisthiazole and their anticancer activities. Heterocycl Commun 7:83–90

17. Miri R, Razzaghi-asl N, Mohammadi MK (2013) QM study and conformational analysis of an isatin Schiff base as a potential cytotoxic agent. J Mol Model 19:727–735
18. Aboul-Fadl T, Mohammed FA-H, Hassan EA-S (2003) Synthesis, antitubercular activity and pharmacokinetic studies of some Schiff bases derived from 1-alkylisatin and isonicotinic acid hydrazide (INH). Arch Pharm Res 26:778–784
19. Narender M, Umasankar K, Malathi J et al (2016) Synthesis, in vitro antimycobacterial evaluation and docking studies of some new 5, 6, 7, 8-tetrahydropyrido [4′, 3′: 4, 5] thieno [2, 3-d] pyrimidin-4 (3H)-one schiff bases. Bioorg Med Chem Lett 26:836–840
20. Junaid M, Alam MJ, Hossain MK et al (2018) Molecular docking and dynamics of Nickel-Schiff base complexes for inhibiting β-lactamase of Mycobacterium tuberculosis. Silico Pharmacol 6:6
21. Salve PS, Alegaon SG, Sriram D (2017) Three-component, one-pot synthesis of anthranilamide Schiff bases bearing 4-amino-quinoline moiety as Mycobacterium tuberculosis gyrase inhibitors. Bioorg Med Chem Lett 27:1859–1866
22. de Souza AO, Galetti F, Silva CL et al (2007) Antimycobacterial and cytotoxicity activity of synthetic and natural compounds. Quim Nova 30:1563–1566
23. Krátký M, Dzurková M, Janoušek J et al (2017) Sulfadiazine salicylaldehyde-based Schiff bases: synthesis, antimicrobial activity and cytotoxicity. Molecules 22:1573
24. Hasan MR, Hossain MA, Salam MA, Uddin MN (2016) Nickel complexes of Schiff bases derived from mono/diketone with anthranilic acid: synthesis, characterization and microbial evaluation. J Taibah Univ Sci 10:766–773. https://doi.org/10.1016/j.jtusci.2015.11.007
25. Uddin MN, Siddique ZA, Mase N et al (2019) Oxotitanium(IV) complexes of some bis-unsymmetric Schiff bases: synthesis, structural elucidation and biomedical applications. Appl Organomet Chem. https://doi.org/10.1002/aoc.4876
26. Frisch MJ, Trucks GW, Schlegel HB et al (2009) Gaussian 09, revision D. 01. Gaussian Inc, Wallingford
27. Gleeson MP, Gleeson D (2009) QM/MM calculations in drug discovery: a useful method for studying binding phenomena? J Chem Inf Model 49:670–677. https://doi.org/10.1021/ci800419j
28. Becke AD (1988) Density-functional exchange-energy approximation with correct asymptotic behavior. Phys Rev A 38:3098–3100. https://doi.org/10.1103/PhysRevA.38.3098
29. Lee C, Yang W, Parr RG (1988) Development of the Colle-Salvetti correlation-energy formula into a functional of the electron density. Phys Rev B 37:785–789. https://doi.org/10.1103/PhysRevB.37.785
30. Kruse H, Goerigk L, Grimme S (2012) Why the standard B3LYP/6-31G* model chemistry should not be used in DFT calculations of molecular thermochemistry: understanding and correcting the problem. J Org Chem 77:10824–10834. https://doi.org/10.1021/jo302156p
31. Azam F, Alabdullah NH, Ehmedat HM et al (2017) NSAIDs as potential treatment option for preventing amyloid β toxicity in Alzheimer's disease: an investigation by docking, molecular dynamics, and DFT studies. J Biomol Struct Dyn 36:1–19
32. Calais J-L (1993) Density-functional theory of atoms and molecules. Int J Quantum Chem 47:101. https://doi.org/10.1002/qua.560470107
33. Pearson RG (1995) The HSAB Principle—more quantitative aspects. Inorganica Chim Acta 240:93–98. https://doi.org/10.1016/0020-1693(95)04648-8
34. Pearson RG (1986) Absolute electronegativity and hardness correlated with molecular orbital theory. Proc Natl Acad Sci 83:8440–8441
35. Berman HM, Westbrook J, Feng Z et al (2006) The protein data bank, 1999–. In: Rossmann MG, Arnold E (eds) International tables for crystallography volume: F: crystallography of biological macromolecules. Springer, New York, pp 675–684
36. Schneidman-Duhovny D, Inbar Y, Nussinov R, Wolfson HJ (2005) PatchDock and SymmDock: servers for rigid and symmetric docking. Nucleic Acids Res 33:W363–W367
37. Mashiach E, Schneidman-Duhovny D, Andrusier N et al (2008) FireDock: a web server for fast interaction refinement in molecular docking. Nucleic Acids Res 36:W229–W232
38. Pettersen EF, Goddard TD, Huang CC et al (2004) UCSF Chimera—a visualization system for exploratory research and analysis. J Comput Chem 25:1605–1612
39. Krieger E, Darden T, Nabuurs SB et al (2004) Making optimal use of empirical energy functions: force-field parameterization in crystal space. Proteins Struct Funct Bioinforma 57:678–683
40. Case DA, Cheatham TE, Darden T et al (2005) The Amber biomolecular simulation programs. J Comput Chem 26:1668–1688
41. Krieger E, Nielsen JE, Spronk CAEM, Vriend G (2006) Fast empirical pKa prediction by Ewald summation. J Mol Graph Model 25:481–486
42. Krieger E, Vriend G (2015) New ways to boost molecular dynamics simulations. J Comput Chem 36:996–1007
43. Cheng F, Li W, Zhou Y et al (2012) admetSAR: a comprehensive source and free tool for assessment of chemical ADMET properties. J Chem Inf Model 52:3099–3105. https://doi.org/10.1021/ci300367a
44. Cohen N, Benson SW (1993) Estimation of heats of formation of organic compounds by additivity methods. Chem Rev 93:2419–2438
45. Garbett NC, Chaires JB (2012) Thermodynamic studies for drug design and screening. Expert Opin Drug Discov 7:299–314. https://doi.org/10.1517/17460441.2012.666235
46. Lien EJ, Guo Z-R, Li R-L, Su C-T (1982) Use of dipole moment as a parameter in drug-receptor interaction and quantitative structure-activity relationship studies. J Pharm Sci 71:641–655. https://doi.org/10.1002/jps.2600710611
47. Saravanan S, Balachandran V (2014) Quantum chemical studies, natural bond orbital analysis and thermodynamic function of 2, 5-dichlorophenylisocyanate. Spectrochim Acta Part A 120:351–364
48. Uzzaman M, Uddin MN (2019) Optimization of structures, biochemical properties of ketorolac and its degradation products based on computational studies. DARU J Pharm Sci 27:1–12
49. Uzzaman M, Shawon J, Siddique ZA (2019) Molecular docking, dynamics simulation and ADMET prediction of Acetaminophen and its modified derivatives based on quantum calculations. SN Appl Sci 1:1437. https://doi.org/10.1007/s42452-019-1442-z
50. Uzzaman M, Hoque MJ (2018) Uzzaman M, Hoque MJ (2018) Physiochemical, molecular docking, and pharmacokinetic studies of Naproxen and its modified derivatives based on DFT. Int J Sci Res Manag. https://doi.org/10.18535/ijsrm/v6i9.c01
51. Politzer P, Murray JS (1990) Electrostatic potential analysis of dibenzo-p-dioxins and structurally similar systems in relation to their biological activities. Adenine press, Schenectady
52. Meroueh SO, Fisher JF, Schlegel HB, Mobashery S (2005) Ab initio QM/MM study of class A β-lactamase acylation: dual participation of Glu166 and Lys73 in a concerted base promotion of Ser70. J Am Chem Soc 127:15397–15407
53. Wang F, Cassidy C, Sacchettini JC (2006) Crystal structure and activity studies of the Mycobacterium tuberculosis β-lactamase reveal its critical role in resistance to β-lactam antibiotics. Antimicrob Agents Chemother 50:2762–2771
54. Feiler C, Fisher AC, Boock JT et al (2013) Directed evolution of Mycobacterium tuberculosis β-lactamase reveals gatekeeper

residue that regulates antibiotic resistance and catalytic efficiency. PLoS ONE 8:e73123
55. Amin ML (2013) P-glycoprotein inhibition for optimal drug delivery. Drug Target Insights 7:27
56. Sanguinetti MC, Tristani-Firouzi M (2006) hERG potassium channels and cardiac arrhythmia. Nature 440:463–469